





RESEARCH ARTICLE | MARCH 17 2022

Propulsive performance of plunging airfoils in biplane configuration

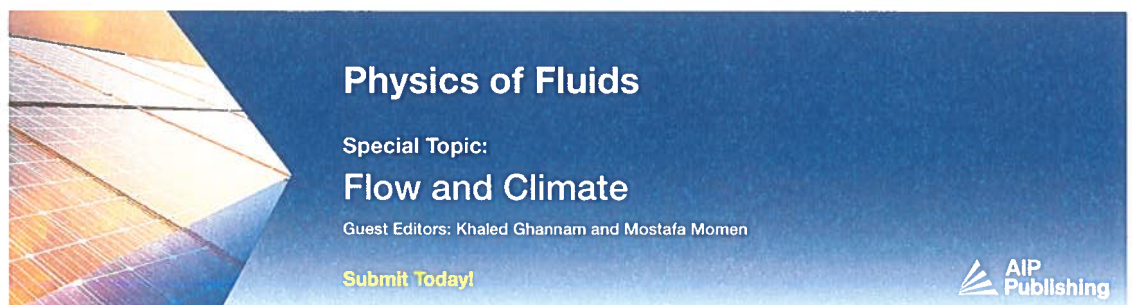
Special Collection: [Flow and Acoustics of Unmanned Vehicles](#)

S. B. Yucel   ; M. Sahin  ; M. F. Unal 


 Check for updates

Physics of Fluids 34, 033611 (2022)

<https://doi.org/10.1063/5.0083040>



Physics of Fluids
Special Topic:
Flow and Climate
Guest Editors: Khaled Ghannam and Mostafa Momen
[Submit Today!](#)



Propulsive performance of plunging airfoils in biplane configuration

Cite as: Phys. Fluids **34**, 033611 (2022); doi: [10.1063/5.0083040](https://doi.org/10.1063/5.0083040)
Submitted: 21 December 2021 · Accepted: 19 February 2022 ·
Published Online: 17 March 2022



S. B. Yucel,^{1,a)} M. Sahin,¹ and M. F. Unal²

AFFILIATIONS

¹Faculty of Aeronautics and Astronautics, Astronautical Engineering Department, Istanbul Technical University, Maslak, Istanbul, 34469, Turkey

²Faculty of Engineering, Mechanical Engineering Department, MEF University, Maslak, Istanbul, 34396, Turkey

Note: This paper is part of the special topic, Flow and Acoustics of Unmanned Vehicles.

^{a)}Author to whom correspondence should be addressed: yucelsa@itu.edu.tr

ABSTRACT

Biplane configuration of pure plunging airfoils is investigated in terms of vortex dynamics both experimentally and numerically by utilizing particle image velocimetry and unstructured finite volume solver of incompressible unsteady Navier–Stokes equations. Experiments are carried out to disclose the vortex shedding and interaction mechanisms for various values of frequency and amplitude of the plunging motion. For the non-dimensional plunge amplitude with respect to the chord of airfoil $h = 0.2$, the effect of the reduced circular frequency based on chord length and the free stream velocity $k = 1$ and 10 are considered, whereas for $h = 0.3$, $k = 2, 4, 8$, and 10 cases are examined. Influence of the plunge amplitude is studied for $h = 0.25$ at $k = 2.5$ and for $h = 0.0875, 0.15$, and 0.3 at $k = 4$. Numerical simulations are performed to investigate the effect of phase difference on vortex structures and propulsive characteristics, such as thrust and Froude efficiency. Two cases having the highest thrust and efficiency values $k = 2.5$, $h = 0.25$, and $k = 4$, $h = 0.15$ value couples are selected for the phase angle of $\phi = 0^\circ$, $\phi = 90^\circ$, $\phi = 180^\circ$, and $\phi = 270^\circ$. Opposed plunge, $\phi = 180^\circ$, was found as the most efficient amongst all phase angles that were investigated, where $\phi = 90^\circ$ is beneficial in lift production. Additionally, three-dimensional simulations indicate no significant three dimensionalities for the parameters used herein.

Published under an exclusive license by AIP Publishing. <https://doi.org/10.1063/5.0083040>

I. INTRODUCTION

In flapping wing aerodynamics, the utilization of multiple wings, especially in biplane configuration, has gained a great deal of interest because of the propulsive superiority over single wing at low Reynolds numbers. In the fixed-wing aircrafts of the early 1900s, biplane configuration of wings is preferred mostly for its structural benefits at the expense of increased drag compared to single wing. In this age, inspired by insect flight, biplane flapping wings are considered as an alternative propulsion system in MAV (Micro Air Vehicle) and MFI (Micro-mechanical Flying Insect) design, due to their enhanced thrust and efficiency values.

To date, many studies were conducted using the principle of pitching/heaving airfoils to produce thrust, known as the Knoller–Betz effect. The utilization of multiple wings became considerably wide spread in the early 2000s. Jones and Platzer¹ investigated single wings as well as the tandem and biplane wing configurations. According to their unsteady panel code analysis, it was observed that biplane configuration was found to be rather promising for thrust production.

In order to investigate ground effect, Jones *et al.*² studied biplane flapping wing propulsion in terms of thrust and efficiency both experimentally and numerically. Using their high aspect ratio model, smoke wire, LDV (laser Doppler velocimetry) and direct thrust measurements both qualitative and quantitative results were obtained. A two-dimensional, unsteady, inviscid panel code and two-dimensional, unsteady Navier–Stokes solver was utilized in their numerical studies. According to their results, a strong Reynolds number dependency is revealed without the advantages of wake interference at Reynolds number on the order of 10^4 . On the other hand, Tuncer and Kaya³ studied airfoils in a biplane arrangement numerically using moving overset grids. They revealed the unsteady flow fields with the help of particle traces and observed that airfoils pitching and plunging in a biplane arrangement with an appropriate phase difference, 20%–40% more thrust is achieved compared with a single airfoil. It is also reported that turbulence in the flow and combined pitching motion provides additional thrust production via prevention of formation of large scale vortices.

In addition to the experimental and numerical studies, flight tests are performed for flapping biplane MAVs. Jones *et al.*⁴ studied the improvement and flight testing of a radio controlled MAV's propulsion system which was composed of a low aspect ratio fixed-wing with a counter-phase flapping trailing pair of higher aspect ratio wings. Like the flight in ground effect, a mechanically and aerodynamically stable platform is provided by the symmetric flapping-wing couple, which increases efficiency and suppresses stall over the main wing by entraining flow. According to their results, the static thrust figure of merit was 60% higher than propellers with a similar scale and disk loading. In addition, Jones and Platzer⁵ summarize the numerical and experimental investigations that lead up to the evolution of authors' flapping wing MAV. They had systematic studies on aerodynamic performance of single and multiple airfoil combinations. It is emphasized that the performance of one surface is closely associated with other surfaces. In their study, it is strongly recommended to discover low-Reynolds number aerodynamics, including unsteady vertical, separated, or three-dimensional flow.

In order to get the best performance, Kaya *et al.*⁶ studied optimizations of aeroelastic flapping airfoils in a biplane arrangement, which are attached to swing arms by an elastic joint. Gradient-based optimization is done by changing the stiffness coefficient and mass moment of inertia of the airfoil for maximum thrust. On moving and deforming overset grids, Navier–Stokes solution for unsteady low speed flows are obtained. They asserted that optimum aeroelastic pitching motion gives more thrust than sinusoidal pitching motion. Also, Kaya *et al.*⁷ studied on the parameter optimization of biplane airfoil configuration in order to get maximum thrust and/or propulsive efficiency. A parallel flow solver on moving and deforming overset grids was used for resolving the unsteady and viscous flow fields around airfoils that is in pitching and plunging motion. For a range of flapping frequencies, sinusoidal pitch, plunge amplitudes, and phase difference between them are optimized. Their results showed that biplane airfoil configuration produced about 25% more thrust than a single airfoil within the Strouhal number range of $0.17 < St < 0.25$, but above this range thrust is decreased dramatically compared to a single airfoil.

For thrust and efficiency augmentation, several studies are done for flexible biplane wing configurations. Dong and Lu⁸ numerically investigated flow over traveling wavy foils in a side-by-side configuration. Similar to the backbone undulation of swimming fish, each foil undergoes lateral motion. Lateral interference is found beneficial for reducing power requirement and for force enhancement. In another study, by utilizing the unsteady panel method, Han, Lee, and Cho⁹ investigated the aerodynamic performance of dual fish like foils in terms of horizontal and vertical spacing. According to their results, vortex–vortex interactions affect the pointing direction of mushroom heads. They state that the total performance mostly depends on horizontal spacing; thus, the strength of mutual interaction is governed by vertical spacing. Miao, Sun, and Tai¹⁰ investigated the effect of chordwise flexible deformation on the aerodynamic features of asynchronously flapping biplane NACA0014 airfoils, for Reynolds numbers of 10^2 , 10^3 , and 10^4 , reduced frequencies from 0.5 to 3.5 and with flexure extent ranging from $0c$ to $0.3c$. Using time-dependent 2D laminar RANS (Reynolds-Averaged Navier–Stokes) equations coupled with conformal hybrid meshes, they visualized particle paths of LEV (leading edge vortex) growth along the airfoil. Their results showed that biplane counter-flapping gives 6.32% more thrust than a rigid single

airfoil. In addition, $0.25c$ flexure extent enhances propulsive efficiency about 64.65% more than biplane rigid airfoils. They stated that proper flexible biplane flapping flight both augments thrust force and propulsive performance, and that the propulsion efficiency is influenced primarily by the value of the reduced frequency rather than by the Reynolds number. On the other hand, in the study of De Clercq *et al.*,¹¹ a flexible biplane flapping-wing MAV was designed and built at Delft University of Technology, DelFly II. It is investigated using PIV (particle image velocimetry) and simultaneous force measurements. It was estimated that in unsteady lift generation, both the clap and peel mechanism and leading edge vortex formation throughout the translational phase are critical for flapping wing motion. According to the PIV results, a powerful influx between the wings was found during the peel but during the clap yet no downward expelling jet. The force measurements show that unlike clap, peel considerably increases the lift. The existence of a leading edge vortex during the first half of the in- and outstroke, which is supported by a simultaneous augmentation in lift, was predicted from the PIV visualization. Similarly, Deng *et al.*¹² studied the propulsive performance of counter-flapping flexible wings in biplane configuration using an in-house code solving compressible unsteady Reynolds averaged Navier–Stokes equation on deforming overset grid. It is stated that biplane arrangement of wings has better propulsive performance compared to single flapping wing, since counter-flapping motion creates a momentum surfeit into the wake and more thrust is generated due to low pressure regime between the wings during outstroke.

For better propulsion, others considered adding a tail to the biplane arrangement. Tay, Hester, and Van Oudheusden¹³ numerically studied the interactions between an upstream biplane airfoil and a stationary tail. They investigated the spacing and the angle of attack of airfoils and its tail on the total propulsion performance. For simulations, an immersed boundary method Navier–Stokes solver is used at Reynolds number 1000. It was shown that total efficiency is increased by 17% and average thrust for each foil is increased up to 126% while two foils are correlated. They also observed that as the vertical spacing between airfoils decreases, especially at $0.122c$, efficiency and thrust coefficient increase. On the contrary, Shen and Cai¹⁴ numerically investigated the biplane arrangement of airfoils together with a stationary tail by employing an URANS (Unsteady Reynolds-Averaged Navier–Stokes) solver coupled with an overset grid method. The tail in the biplane configuration is considered as inefficient.

Several other studies considered spacing of airfoils. Bao *et al.*¹⁵ computationally studied the performance of two antiphase pitching airfoils in biplane arrangement. Their aim is to investigate the effect of the vertical gap (g) between the airfoils and Strouhal number-based pitching amplitude (St_A). It is asserted that compared to isolated airfoil, biplane arrangement has 37.6% higher propulsion efficiency for $St_A = 0.28$ and $g = 1.0D$ and also decreasing gap results in earlier drag to thrust transition at smaller Strouhal number. In particular, higher efficiency is related to the type of the wake being a unitary jet like flow or two parallel vortex streets. In another study, Zhu and Lei¹⁶ investigated two counter-flapping airfoils numerically, doing combined pitching and plunging motion. Their aim was to investigate the effect of phase angle in pitch motion and the effect of spacing between airfoils. The performance of biplane arrangement is found to be better when compared with single flapping wing due to wing-wing interaction. It is argued that the biplane counter-flapping wing with proper

mean wing to wing distance has better performance because of stronger and larger vertical distance of vortices that are formed. Additionally, the unsteady aerodynamics of multi-plunging ellipsoidal airfoils are studied computationally by Amiralaie, Alighanbari, and Hashemi,¹⁷ showing the importance of airfoil interactions. Reynolds number, frequency, and amplitude of oscillations are all found to be effective on the aerodynamic performance of airfoils.

Pitching motion of the airfoils in biplane configuration continue to receive attention in more recent studies. Numerical simulation of flow around pitching airfoils in biplane configuration by Gungor, Khalid, and Hemmati¹⁸ reveals several unsteady wake modifications due to abrupt changes in phase angle between them. Zhu and Zhang¹⁹ also numerically examine the pitching motion of a pair of NACA0015 airfoils at biplane configuration. These semi-active pitching airfoils are arranged as an energy extraction mechanism to perform forced counter-pitching motion and are subsequently induced in a plunging motion. The results show that the biplane configuration of the semi-active pitching airfoils is beneficial for the power extraction efficiency of the airfoil rather than the power absorbed from the fluid.

As the brief summary of the related literature above indicates, majority of studies on airfoils in biplane arrangement considers the pitching or combined pitching and plunging motions. The study herein focuses on the pure plunging motion of a pair of NACA0012 airfoils in biplane arrangement. Extensive flow field measurements with DPIV (Digital Particle Image Velocimetry) are augmented with numerical simulations. Utilization of arbitrary Lagrangian–Eulerian (ALE) method in numerical simulations has been beneficial in solving large deflections accurately and using the minimum distance function from the airfoil surface for large mesh deformation provided numerical efficiency. With the potential application areas of bio-inspired vehicles and energy harvesting systems due to oscillations of airfoils induced by fluid structure interactions, the objective of the study is to provide insight into the complex vortex interactions, wake structures and propulsive characteristics of the biplane airfoils for several reduced frequencies and non-dimensional plunge amplitudes at Reynolds number 2000. Additionally, the effect of phase difference between airfoils is investigated in detail regarding thrust and efficiency values, as well as vorticity structures via numerical simulations for $\phi = 0^\circ$, $\phi = 90^\circ$, $\phi = 180^\circ$, and $\phi = 270^\circ$ which have not been reported in related literature to date.

II. METHODS

A. Experimental procedure

In the experimental phase of the study, two Plexiglas NACA0012 wing models with 100 mm chord and 300 mm wingspan are used in a large-scale water channel available at the Trisonic Laboratory of the Faculty of Aeronautics and Astronautics, Fig. 1. The cross-sectional dimensions of the main test section of the channel are 1010 mm \times 790 mm. The channel has a settling reservoir and honeycomb-screen arrangements in order to maintain low turbulence intensity, which is less than 1%. The maximum velocity of the water channel at 710 mm water level is 0.13 m/s. The plunging motion is performed with two Kollmorgen/Danaher Motion AKM33E servo motors and their gear systems. The flow is illuminated by a dual cavity Nd:Yag laser and the water is seeded with silver coated hollow glass spheres of 10 μ m mean diameter. The flow images are captured by two 10 bit flow sense cameras with 1,600 \times 1,200 pixels resolution and 30 Hz frame rate.

B. Numerical algorithm

The integral form of the incompressible Navier–Stokes equations that govern the motion of an arbitrary moving control volume $\Omega(t)$ with boundary $\partial\Omega(t)$ can be written in the Cartesian coordinate system in dimensionless form as follows: the continuity equation,

$$-\oint_{\partial\Omega} \mathbf{n} \cdot \mathbf{u} dS = 0, \quad (1)$$

the momentum equation,

$$Re \int_{\Omega} \frac{\partial \mathbf{u}}{\partial t} dV + Re \oint_{\partial\Omega} [\mathbf{n} \cdot (\mathbf{u} - \dot{\mathbf{x}})] \mathbf{u} dS + \oint_{\partial\Omega} n p dS = \oint_{\partial\Omega} \mathbf{n} \cdot \nabla \mathbf{u} dS. \quad (2)$$

In these equations, V is the control volume, S is the control volume surface area, \mathbf{n} represents the outward normal vector, \mathbf{u} represents the local fluid velocity vector, $\dot{\mathbf{x}}$ represents the grid velocity, p is the pressure, and Re is the Reynolds number. The above governing equations are discretized using the unstructured side-centered finite volume method based on an arbitrary Lagrangian–Eulerian (ALE) formulation given in detail in Erzincanli and Sahin.²⁰ In this approach, the velocity vector components are defined at the mid-point of each cell face, while the pressure term is defined at element centroids. The present arrangement of the primitive variables leads to a numerically stable scheme and it does not require any *ad hoc* modifications in order to remove the checker-board pressure oscillations arising from the pressure-velocity decoupling. In the current discretization, the conservation is satisfied within each quadrilateral/hexahedral elements at machine precision and the summation of the discrete equations can be exactly reduced to the domain boundary, which is important for the global mass conservation. In addition, a particular attention is given to develop a second-order arbitrary Lagrangian–Eulerian algorithm obeying the discrete geometric conservation law (DGCL).²¹ The resulting large-scale algebraic linear systems are solved in a fully coupled manner using the FGMRES (Flexible Generalized Minimal Residual method) Krylov iterative method²² preconditioned with a matrix factorization similar to that of the projection method²³ for the whole system and the parallel algebraic multigrid solver BoomerAMG is used for the scaled discrete Laplacian provided by the HYPRE (A Library of High Performance Preconditioners) library²⁴ which we access through the PETSc library²⁵ developed at the Argonne National Laboratories for improving the efficiency of the parallel code. The METIS (Unstructured Graph Partitioning and Sparse Matrix Ordering System) library²⁶ is used to partition the computational domain into sub-domains for a balanced domain decomposition. Although the ALE algorithm uses indirect radial basis function (RBF) algorithm for large mesh deformation, in the current work the mesh motion algorithm is based on an algebraic method using the minimum distance function from the airfoil surface due to its numerical efficiency. The outer boundary conditions are set to the free-stream values except at the outflow where the natural (traction-free) boundary condition is used. The boundary condition on the airfoil surface is set to no-slip. As the initial flow conditions, the present calculations are impulsively started from rest. The present ALE algorithm has been validated for the decaying Taylor–Green vortex flow, the flow past an oscillating circular cylinder in a channel and the flow induced by an oscillating sphere in a cubic cavity.²⁰ The numerical method has also been

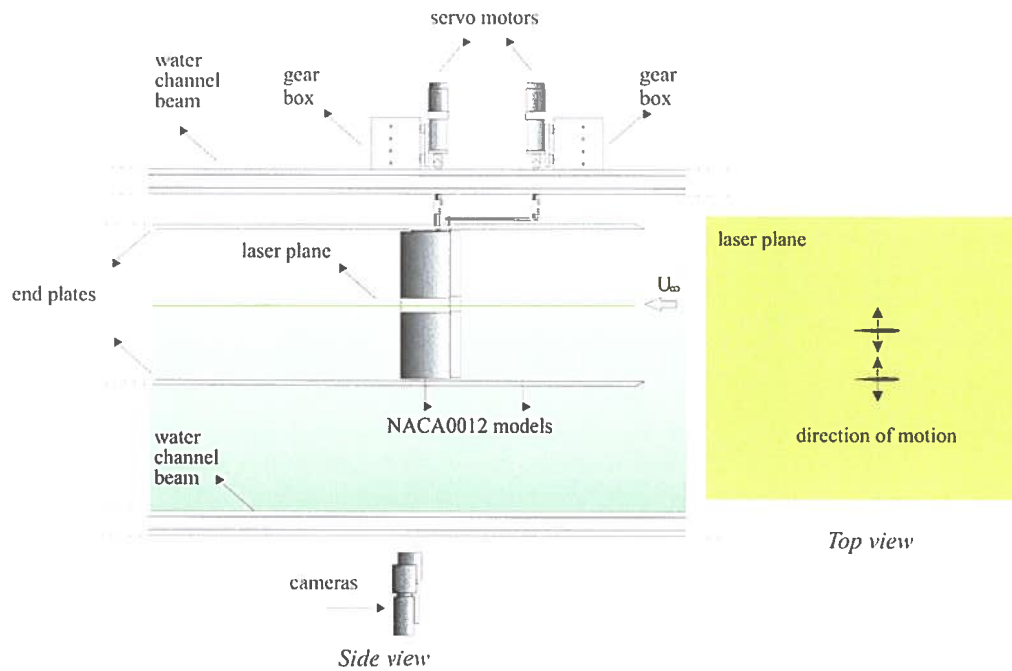


FIG. 1. Experimental apparatus.

successfully used to simulate the purely viscoelastic wake instabilities behind a confined circular cylinder for the first time.^{27,28}

The magnitude of the total forces acting on the NACA0012 airfoil and the total power requirement are computed from the following surface integrals as a function of time:

$$\mathbf{F}(t) = \oint_{\partial\Omega} (\mathbf{n} \cdot \boldsymbol{\sigma}) dS, \quad (3)$$

$$P(t) = \oint_{\partial\Omega} \mathbf{n} \cdot (\boldsymbol{\sigma} \cdot \mathbf{u}) dS, \quad (4)$$

where $\boldsymbol{\sigma}$ is the stress tensor including the pressure term, $(\mathbf{n} \cdot \boldsymbol{\sigma})$ is the traction vector, and $\partial\Omega$ is the airfoil surface. The computed force and power coefficients as well as the efficiency of the NACA0012 airfoil are calculated, respectively, as

$$C_f = \frac{F}{0.5\rho U_\infty^2 S}, \quad (5)$$

$$C_p = \frac{P}{0.5\rho U_\infty^3 S}, \quad (6)$$

$$\eta_E = \frac{\langle F_x \rangle U_\infty}{\langle P \rangle}, \quad (7)$$

where U_∞ is the free stream velocity, $\langle F_x \rangle$ is the thrust, and $\langle P \rangle$ is the required power. The vertical plunge motions of the NACA0012 airfoils with a frequency of f are given by

$$y_{upper}(t) = h \sin(2\pi ft), \quad (8)$$

$$y_{lower}(t) = -h \sin(2\pi ft), \quad (9)$$

where h is the non-dimensional plunge amplitude with respect to the airfoil chord length. The Reynolds number $Re = U_\infty c / \nu$ based on the airfoil chord length c and the kinematic viscosity ν . The non-dimensional reduced frequency k is defined to be $2\pi fc / U_\infty$ and the period of the vertical plunge motion is given by $T = 2\pi c / k U_\infty$. For the rest of the study, Reynolds number is kept constant as 2000, and vertical distance between the airfoils is $1c$ unless otherwise stated.

III. RESULTS

A. Mesh dependency and validation

Mesh dependency analysis is done for a plunging single airfoil, using parameters $k=4$ and $h=0.15$ at Reynolds number 2000. Numerical simulations are performed for three conforming mesh sizes, such as M1, M2, and M3, which correspond to the numbers of elements of 99, 150, 399, 244, and 1 609 845. The grid around leading edge is shown in Fig. 2(a). Phase diagram of forces and vorticity contours are presented in Figs. 2(b) and 3, respectively. Both vorticity contours and force results are quite compatible with each other. Therefore, for the rest of the study, the number of elements is kept in between M2 and M3, which is optimum for accuracy (0.5%–0.1% error), with a reasonable computational time. For single wing cases, mesh contains 747 597 quadrilateral elements and for biplane configuration the mesh consisted of 659 198 quad elements where the airfoils are separated one chord apart from each other vertically. The boundary layer grid is created using Gambit 2.1.6 software and the rest of the grid is generated via Cubit 9.1 software using mapping and paving algorithms²⁹ within a domain of $[-10c, 20c] \times [-10c, 10c]$ where the airfoil leading edge is located at the origin. Computational domain, grid, and placement of airfoils in biplane arrangement can be viewed in Fig. 4.

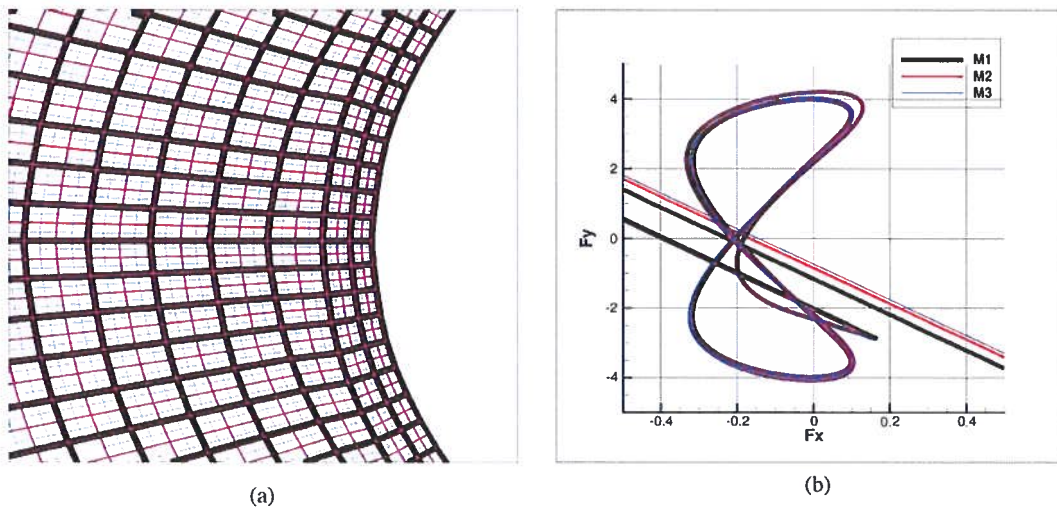


FIG. 2. Mesh structures as M1, M2, and M3 for single airfoil (a) conforming grid from coarse to fine and (b) phase portrait of aerodynamic forces.

The numerical results are validated with experimental findings for the same parameters, which are used to show mesh dependency and represented in Fig. 5. From left to right, a period of vortex shedding is illustrated corresponding to the time values of 0 , $0.25T$, $0.5T$, and $0.75T$. As can be inferred from comparison of the experimental and numerical results, even though there are slight differences in the wake patterns, main flow structures are similar. Some small dissimilarities are mainly due to the lower grid resolution in the experiments when compared to the quite fine numerical grid. Since no force measurement is done during the experimental phase, only qualitative data are available for comparison.

B. Experimental results

Experiments were carried out for a number of $k-h$ parameter pairs to study the effects of reduced frequency (k) and the non-dimensional plunge amplitude (h) for the biplane configuration. The parameters for

the biplane configuration are chosen based on previous findings on vortex wake characteristics of a single plunging airfoil at $Re=2000$. For the single airfoil, based on the master's thesis study of Percin,³⁰ thrust and drag producing cases are indicated in Fig. 6, along with five particular cases indicated as C1–C5 approximately along the boundary between the drag and thrust producing wake $k-h$ value regions. The parameters chosen are centered around C2 ($k=2.5$, $h=0.25$) and C3 ($k=4$, $h=0.15$), since the shedding characteristics alter significantly passing from one case to the other. In doing this, the plunge amplitude is increased to the extent permitted by the experimental setup without the risk of collision of the airfoils.

1. Effect of reduced frequency

In order to investigate the effect of reduced frequency experimentally, two scenarios are considered; low plunge amplitude $h=0.2$ and

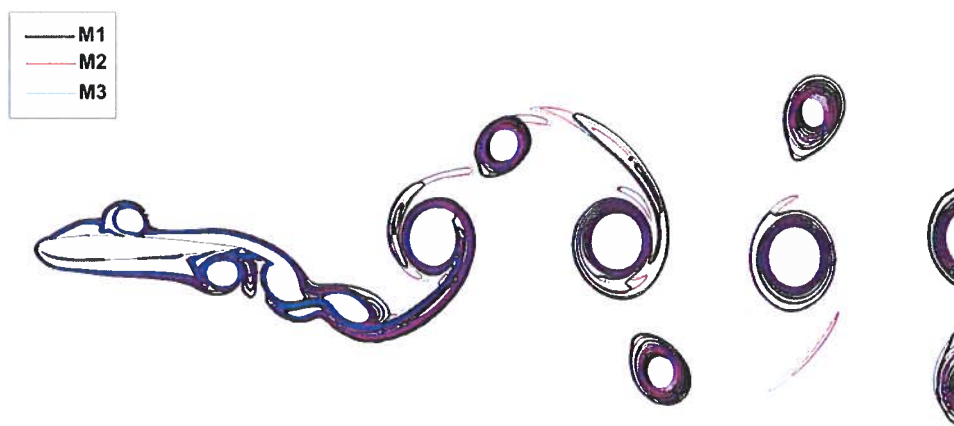


FIG. 3. The computed vorticity contours for M1, M2, and M3.

15 September 2024 11:16:52

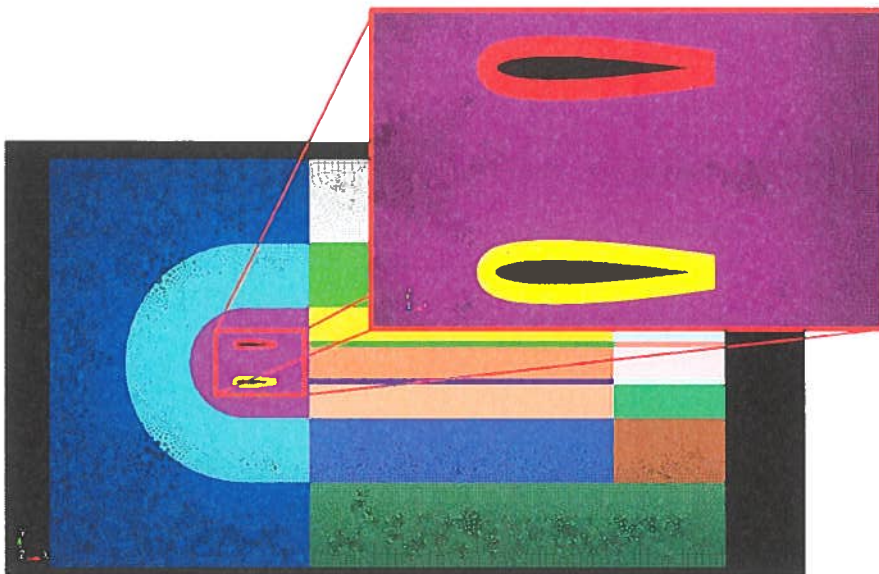


FIG. 4. Computational domain and grid used for biplane configuration.

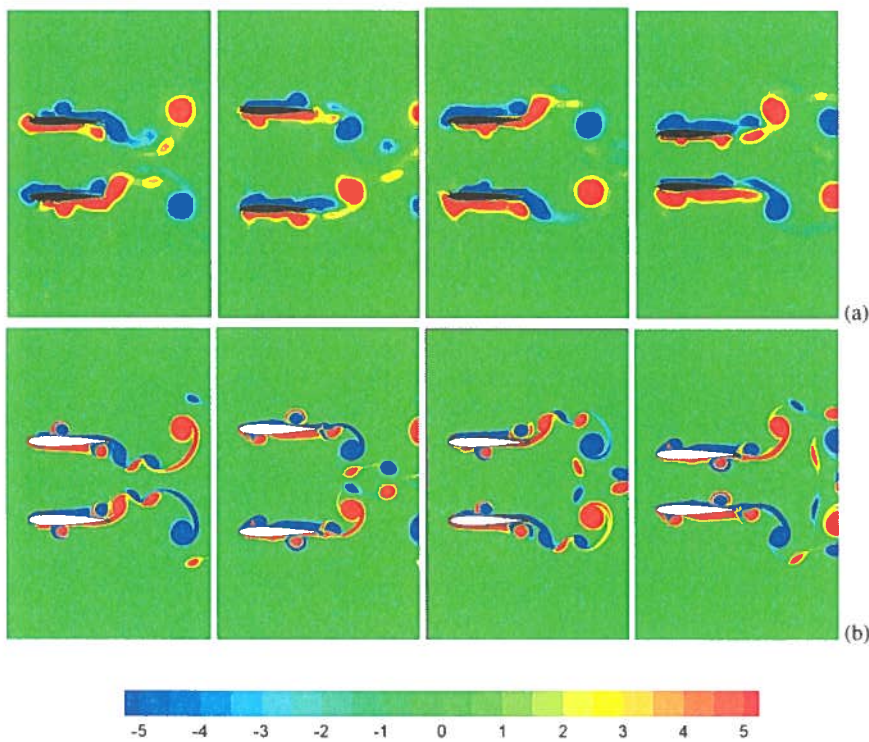


FIG. 5. Vorticity contours; experimental (a) and numerical (b) results for $k = 4$, $h = 0.15$. A period is represented from left to right, corresponding to time values of 0, 0.25T, 0.5T, and 0.75T.

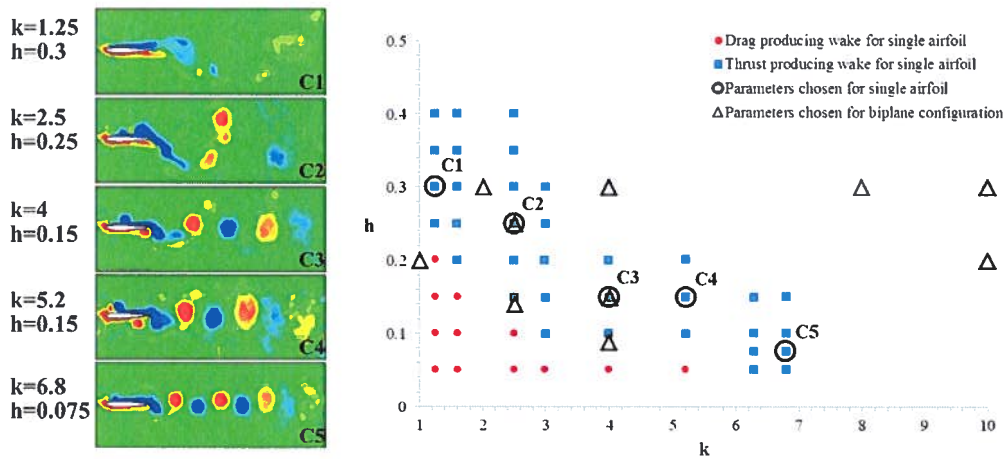


FIG. 6. Parameters chosen (triangles) to study the effects of reduced frequency (k) and non-dimensional plunge amplitude (h) for the biplane configuration. Drag and thrust producing cases for single airfoil are indicated with circles and squares respectively, while the k and h parameter pairs corresponding to the vortex wakes of single airfoil on lhs are indicated as C1, C2, C3, C4, and C5.

high plunge amplitude, $h = 0.3$. Since the initial distance between the wings is one chord, plunge amplitude is no further increased to avoid collision of wings during opposed motion.

For the low amplitude case where $h = 0.2$, reduced frequencies are chosen as $k = 1$ and $k = 10$, which are close to the lower and the upper limits of the experimental setup. Instantaneous vorticity structures are shown in Fig. 7. In upper row where $k = 1$, since the wake is

weak and narrow the two wakes are apart from each other and show no sign of interaction. Hence, the type of wake is similar to that of drag producing Kármán street in domination of trailing edge (TE) vortex. However, for $k = 10$, as shown in lower row of Fig. 7, there exists much stronger leading and trailing edge vortices. The leading edge (LE) vortices are circumnavigate around the leading edge instead of traveling downstream. Therefore, wake type is determined mainly

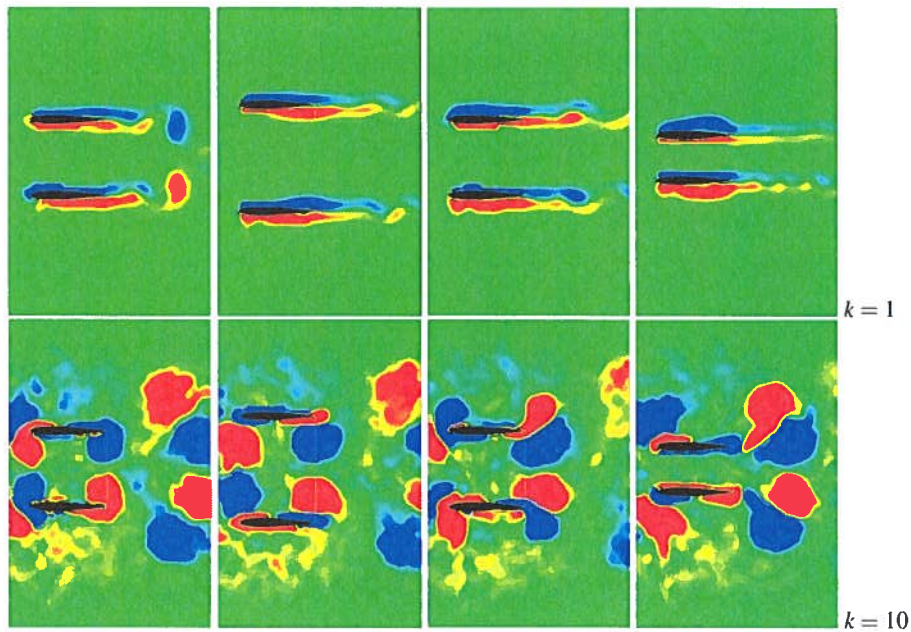


FIG. 7. Experimental vorticity contours for $h = 0.2$, corresponding to reduced frequencies of $k = 1$ (top) and $k = 10$ (bottom). A period of motion is represented from left to right, corresponding to time values of 0, 0.25T, 0.5T, and 0.75T.

15 September 2024 11:16:52

by TE vortices. These TE vortices form vortex pairs which help to generate jet like flow in the wake and enhance thrust generation.

On the other hand, for higher plunge amplitude case where $h = 0.3$, the effect of reduced frequency is investigated in detail with smaller intervals, namely, $k = 2$, $k = 4$, $k = 8$, and $k = 10$ and vorticity contours are illustrated in Fig. 8. As the reduced frequency increases,

vorticity structures are getting larger and stronger especially up to $k = 8$. There is a slight change passing from $k = 8$ to $k = 10$. Additionally, for $k = 2$ vortex shedding mechanism is different from those of $k = 4$, 8 , and 10 with regard to LE and TE vortex shedding mechanisms. Wake is dominated mainly by LE and TE vortices for $k = 2$ whereas for $k = 4$ and higher frequencies LE vortex

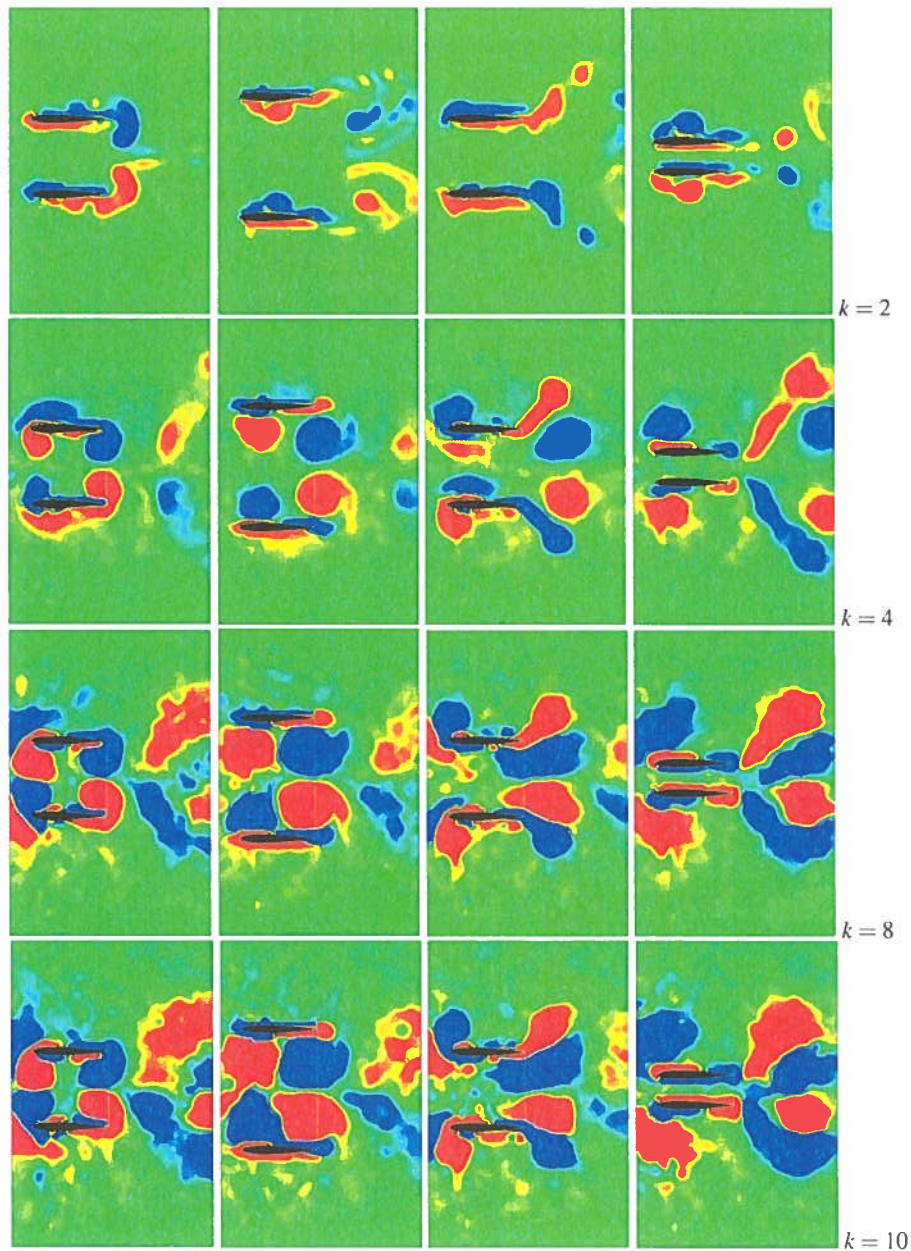


FIG. 8. Experimental vorticity contours for $h = 0.3$, corresponding to reduced frequencies of $k = 2$ (top), $k = 4$, $k = 8$, and $k = 10$ (bottom). A period of motion is represented from left to right, corresponding to time values of 0 , $0.25T$, $0.5T$ and $0.75T$.

circumnavigates around the leading edge and hence wake is dominated mainly by TE vortices. The existence of strong and attached LE vortices expected to provide positive effect on efficiency. For $k = 4$ and higher frequencies, during upstroke motion where airfoils move apart from each other, oppositely signed vortices are formed on both leading and trailing ends of airfoils. These large vortices are sucked into the area between the wings until the beginning of downstroke motion. During the downstroke motion where airfoils move toward to each other, TE vortices are pumped downstream, forming vortex couples whereas major part of LE vortices remain around the leading edges. In the cases of $k = 8$ and $k = 10$ since more energetic vortices are existent, upper and lower airfoils' wakes start interacting with each other and the general flow pattern becomes less symmetrical. Additionally, for reduced frequencies $k = 8$ and $k = 10$ the wake width is decreased when compared to $k = 4$ at $t = 0$ and $t = 0.75T$.

2. Effect of non-dimensional plunge amplitude

In order to determine the effect of plunge amplitude experimentally, using the same approach in investigating the effect of reduced frequency, two scenarios are considered, at low and high reduced frequencies, $k = 2.5$ and $k = 4$, respectively. As shown in Figs. 9 and 10, for increasing plunge amplitude, vorticity magnitudes both from the LE and TE increase regardless of the reduced frequency. Additionally, with increasing plunge amplitude, stronger vortices form at the leading and trailing edges of the airfoils. For $k = 2.5$ and $h = 0.25$, strong vortices apparent around the leading edges in Fig. 9 bottom row are expected to provide a positive effect on the thrust efficiency due to their induced negative pressure, during both upstroke and downstroke motions. Additionally, these LE vortices during upstroke effectively

narrow the gap between the airfoils and thus are expected to be commensurate with speed increase and accompanying suction between the airfoils. For the high frequency case where $k = 4$, LE vortices travel downstream and interact with TE vortices for $h = 0.0875$ and $h = 0.15$, whereas for $h = 0.3$ majority of LE vortices navigate around leading edge as evident in Fig. 10. Additionally, as seen in Fig. 10 bottom row, for $h = 0.3$, large scale TE vortices inside the gap area eventually form vortex dipoles with counter-rotating TE vortices in directions inclined w.r.t. the freestream nearby the TE of the upper and lower airfoils.

To augment these experimentally observed wake dynamics in order to better understand the thrust and efficiency characteristics, numerical simulations are performed for a parameter space indicated in Fig. 11. In this figure, hollow circles stand for drag and negative efficiency values whereas full circles correspond to thrust and positive efficiency values. These findings are compatible with above summarized experimental findings. Among the cases considered, the highest thrust and efficiency for the biplane configuration are obtained for $k = 2.5$, $h = 0.25$. When compared with the single airfoil, the thrust is 53% and efficiency value is 15% higher for this biplane case.

C. Numerical simulation results

1. Effect of phase difference

In order to investigate the effect of phase difference between airfoils, two cases are selected as having the highest thrust and efficiency values as, $k = 2.5$, $h = 0.25$, and $k = 4$, $h = 0.15$, among the parameter space given in Fig. 11. For these sets, considered phase angles are $\phi = 0^\circ$, $\phi = 90^\circ$, $\phi = 180^\circ$, and $\phi = 270^\circ$, in addition to stationary

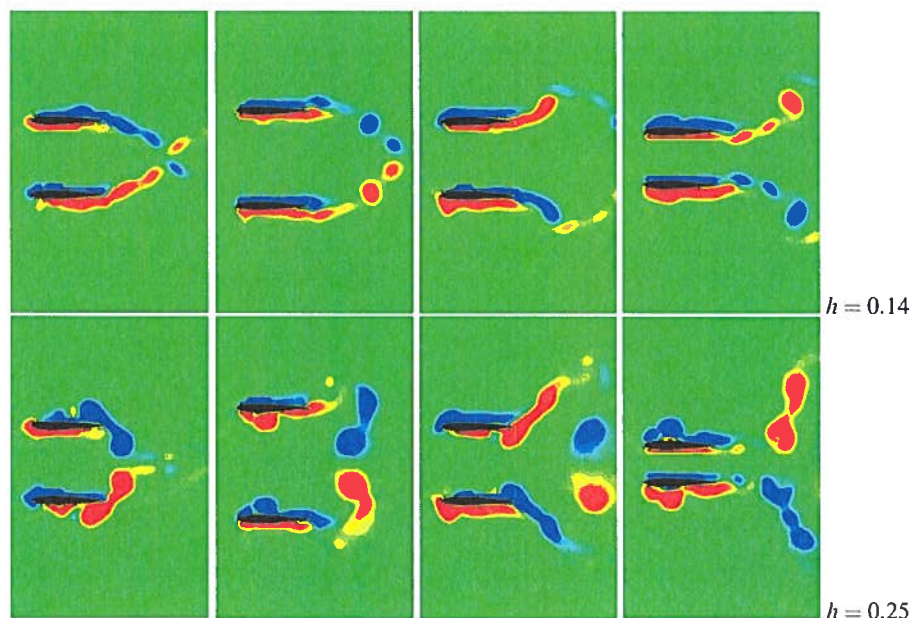


FIG. 9. Experimental vorticity contours at $k = 2.5$, for non-dimensional plunge amplitudes of $h = 0.14$ (top), $h = 0.25$ (bottom). A period is represented from left to right, corresponding to time values of 0, 0.25T, 0.5T, and 0.75T.

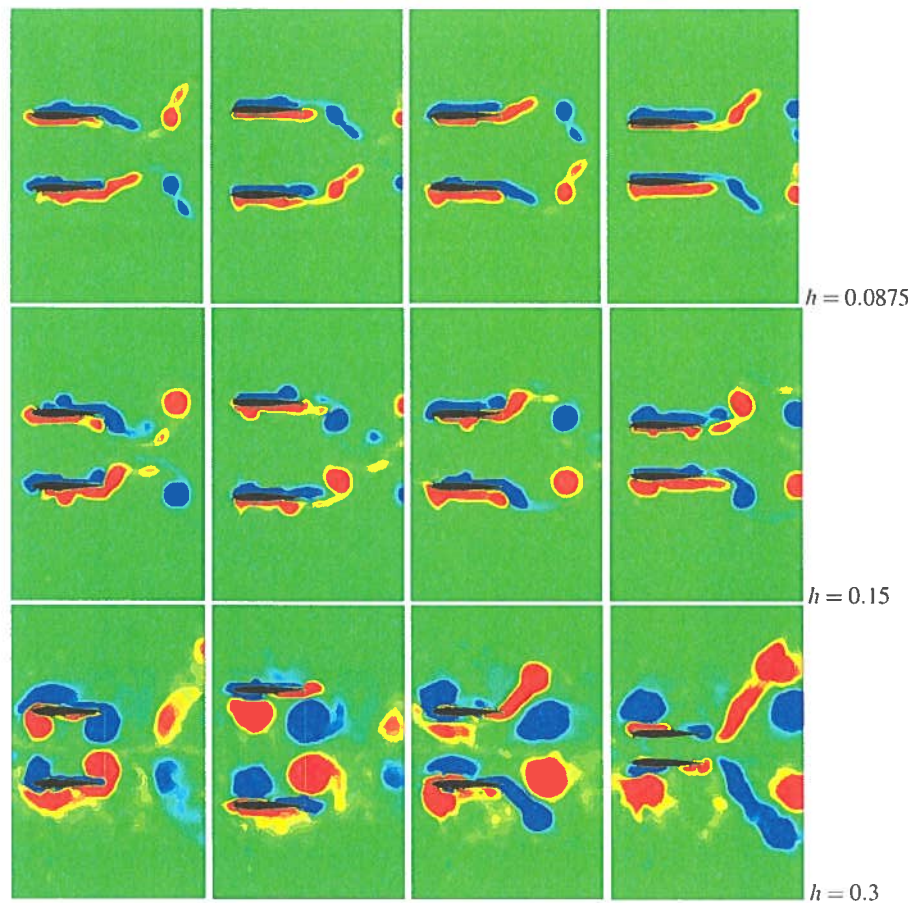


FIG. 10. Experimental vorticity contours at $k = 4$, for non-dimensional plunge amplitudes of $h = 0.0875$ (top), $h = 0.15$ (middle), $h = 0.3$ (bottom). A period is represented from left to right, corresponding to time values of 0, 0.25T, 0.5T, and 0.75T.

lower wing case. For all cases, lift, thrust and power coefficients as well as efficiency values are calculated for lower and upper airfoils and given in Table I. When the average values of upper and lower airfoil values is compared with single airfoil, highest thrust and efficiency is obtained for $\phi = 180^\circ$ where airfoils are in opposed plunge, even though the power coefficient is increased and is the highest of all. In the case of $\phi = 0^\circ$ which means airfoils are moving synchronously, for both k - h pairs thrust and efficiency values decrease. However, at phase angles of $\phi = 90^\circ$ and $\phi = 270^\circ$, for $k = 2.5$, $h = 0.25$ case thrust and efficiency values remains nearly the same whereas for $k = 4$, $h = 0.15$ case there is slight increase. Additionally, for these phase angles there is a force increase in the direction of lift. Also the force statistics on upper and lower airfoils are nonsymmetrical. On the other hand, in the case of biplane with stationary lower wing thrust is decreased in both cases.

Specifically, for all the cases considered, thrust and efficiency values are compared in the histograms of Fig. 12. Similarity is evident between the cases for $k = 2.5$, $h = 0.25$ and $k = 4$, $h = 0.15$. For both

cases, the phase angle $\phi = 180^\circ$ produces higher thrust and efficiency values with respect to single airfoil.

To understand the flow structure and interactions, vorticity contours of $k = 2.5$, $h = 0.25$ (left column) and $k = 4$, $h = 0.15$ (right column) are compared in Fig. 13, where first row stands for single airfoil as reference. Since reduced frequency is higher and plunge amplitude is lower for $k = 4$, $h = 0.15$ case, wake is narrower than $k = 2.5$, $h = 0.25$. In the stationary lower wing scenario, for both k - h values, wake of the upper airfoil is pushed up and slightly modified by the action of the lower airfoil. Since lower airfoil is stationary and drag producing, overall thrust slightly decreases with respect to single airfoil. At $\phi = 0^\circ$ phase angle, Fig. 13(c), where airfoils are moving synchronously vortex pairs merge and form a single row of vortices as they travel further downstream. On the contrary, at $\phi = 180^\circ$ phase angle, Fig. 13(e), where airfoils are moving asynchronously, counter-rotating vortex couples are apparent, and especially recognizable for $k = 4$, $h = 0.15$. Additionally, the wake structures from upper and lower airfoils are of mirror image of each other, similar to a single

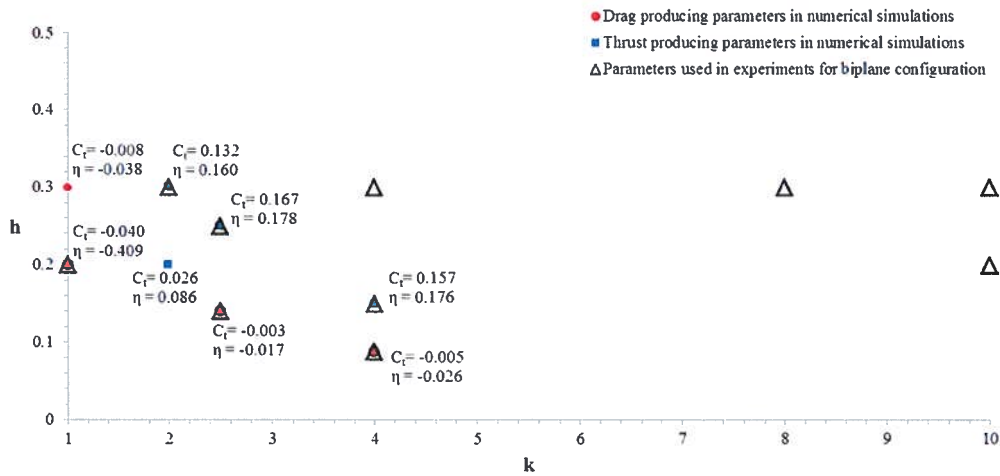


FIG. 11. Parameter space for biplane configuration, together with thrust coefficient and efficiency values obtained from the numerical simulations.

airfoil with ground effect passing through the centerline of the airfoils. With their self-induced velocities, counter-rotating vortex pairs from the trailing edges move toward the gap between plates in the near wake region and away from the centerline further downstream. As a comparison of Figs. 13(d) and 13(f) reveals, for $\phi = 270^\circ$ phase angle, far wake is similar to that of $\phi = 90^\circ$, in that the wake structure in one of the cases is the mirror image of the other.

2. Three dimensionality

To understand the validity of the two dimensional analysis in disclosing the vortex dynamics of plunging airfoils, three dimensionality is investigated for the cases that are used formerly in phase angle effect as $k = 2.5, h = 0.25$ and $k = 4, h = 0.15$. The computational grid consists

of 5 396 717 nodes and 5 188 788 elements. There are 55 elements on wing along the span where domain depth is $0.5c$ in z -direction. The phase angle is chosen as $\phi = 180^\circ$, i.e., opposed plunge, where thrust and efficiency are the highest of all the phase angles considered. The vorticity iso-contours are shown in Fig. 14(a). The results are similar with the ones found in two dimensional calculations, Fig. 13(e). On the other hand, the existence of mild three dimensionality is apparent from the z -velocity contours that are illustrated in Fig. 14(a) (maximum z -velocity value is $0.17m/s$). Specifically, for the $k = 4, h = 0.15$ case, Fig. 14(b) on the right column, the z -velocity is negligible even it is multiplied by the scale factor of 10. In addition, F_x, F_y time histories of 2D and 3D solutions nearly coincides, as presented in Fig. 15. Therefore, having no significant 3D effects, the 2D analysis is proven to be valid to explain the vortex dynamics of plunging airfoils.

TABLE I. Force statistics within mean of eight periods of plunging motion.

		$k = 2.5, h = 0.25$				$k = 4, h = 0.15$			
		C_l	C_d	C_p	η	C_l	C_d	C_p	η
Single		-0.001	0.109	0.710	0.154	-0.002	0.109	0.691	0.158
Stationary lower wing	L ^a	0.013	-0.081	0.000	$-\infty$	0.023	-0.085	0.000	$-\infty$
	U ^b	0.084	0.109	0.734	0.148	0.012	0.110	0.708	0.155
$\phi = 0^\circ$	L	0.403	0.067	0.573	0.117	0.392	0.073	0.546	0.135
	U	-0.404	0.067	0.573	0.117	-0.396	0.073	0.545	0.135
$\phi = 90^\circ$	L	0.284	0.087	0.695	0.125	0.242	0.097	0.740	0.131
	U	-0.093	0.135	0.768	0.176	-0.151	0.129	0.650	0.199
$\phi = 180^\circ$	L	-0.283	0.167	0.942	0.178	0.126	0.157	0.890	0.176
	U	0.283	0.167	0.942	0.178	-0.126	0.157	0.890	0.176
$\phi = 270^\circ$	L	0.093	0.135	0.768	0.177	0.152	0.129	0.650	0.199
	U	-0.283	0.087	0.695	0.125	-0.241	0.097	0.740	0.131

^aLower wing.
^bUpper wing.

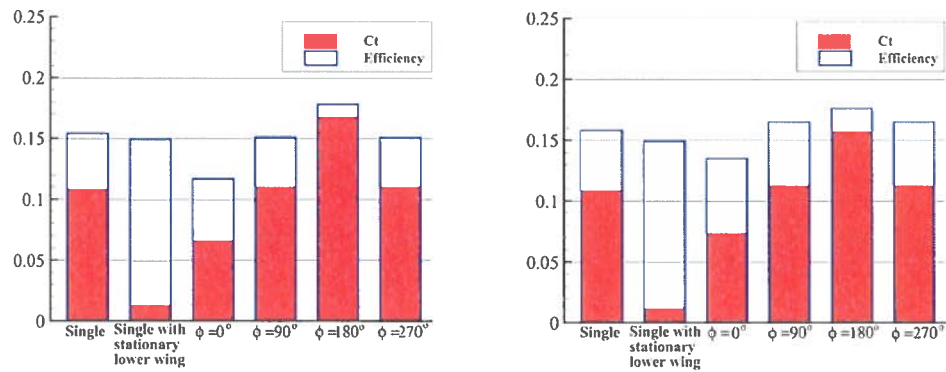


FIG. 12. Comparison of thrust coefficient and efficiency values from numerical simulations for (left) $k = 2.5, h = 0.25$ and (right) $k = 4, h = 0.15$.

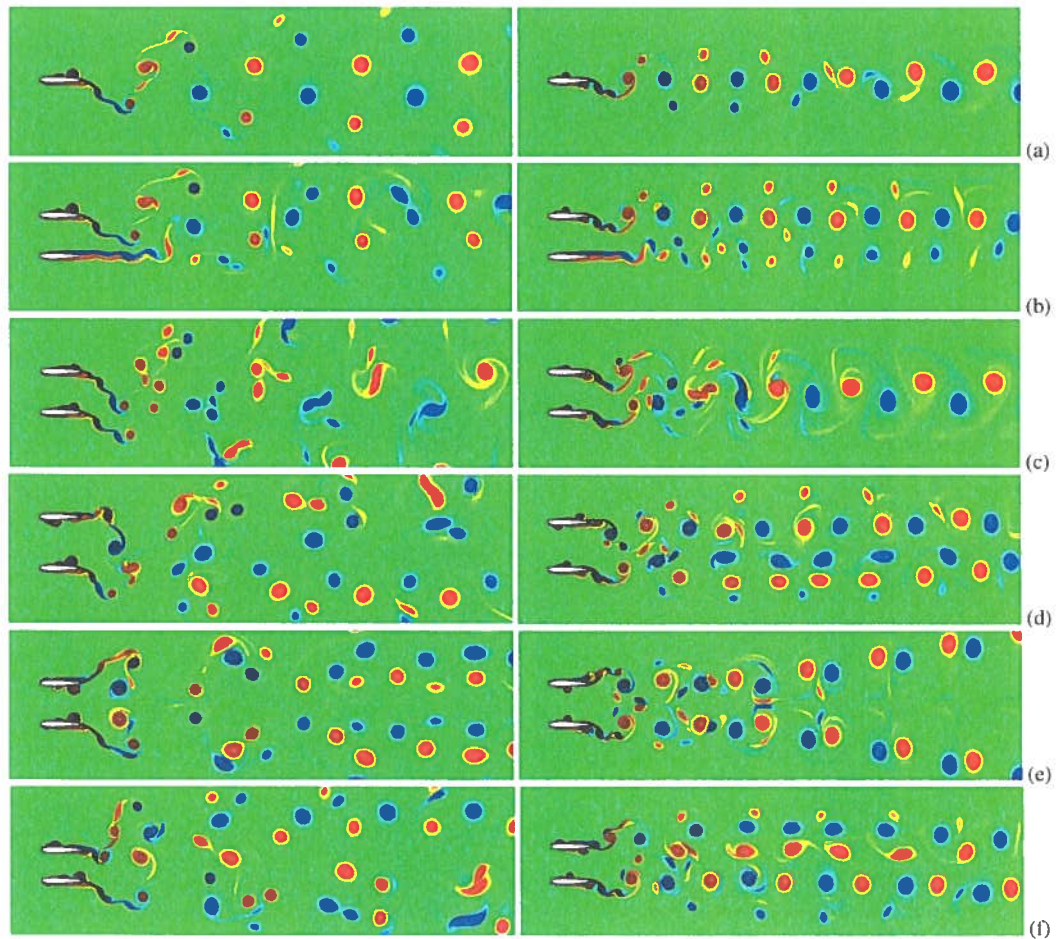


FIG. 13. Instantaneous vorticity contours for $k = 2.5, h = 0.25$ (left) and $k = 4, h = 0.15$ (right), representing (a) single, (b) single with stationary lower wing and phase difference of (c) $\phi = 0^\circ$, (d) $\phi = 90^\circ$, (e) $\phi = 180^\circ$, and (f) $\phi = 270^\circ$.

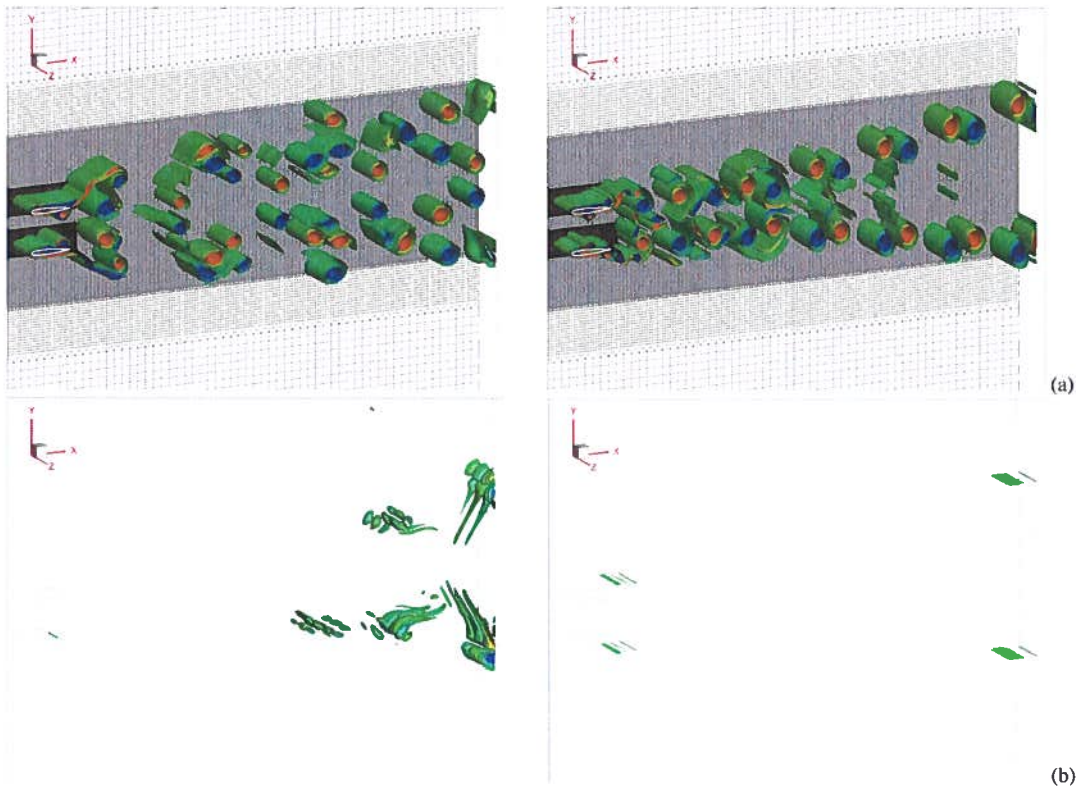


FIG. 14. Iso-surfaces for $k = 2.5, h = 0.25$ (left), and $k = 4, h = 0.15$ (right) at $t = 17.5T$, representing (a) vorticity, (b) z -velocity at phase difference of $\phi = 180^\circ$.

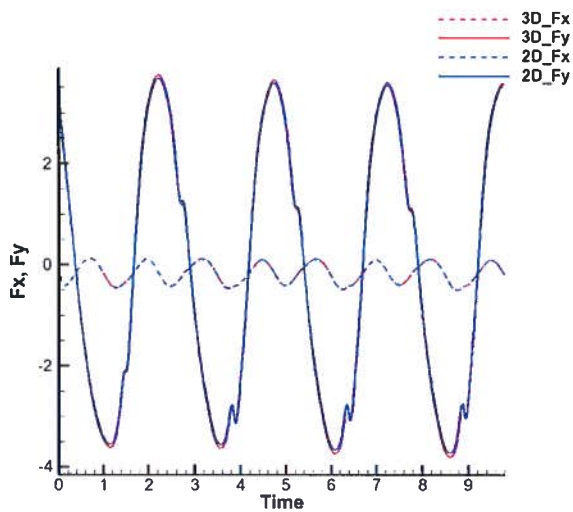


FIG. 15. Comparison of phase diagrams for 2D and 3D for $k = 2.5, h = 0.25$.

IV. CONCLUSIONS

In the current work, pure plunging motion of NACA0012 airfoils in biplane configuration is investigated experimentally by using particle image velocimetry and numerically by solving incompressible unsteady Navier–Stokes equations utilizing arbitrary Lagrangian–Eulerian formulation. The experimental results show that reduced frequency and plunge amplitude alter the flow characteristics significantly. The interacting vortex wakes from the upper and lower airfoils are either leading edge or trailing edge dominated. Generation of counter-rotating vortex pairs behind the plunging airfoils effectively increases the thrust and propulsive efficiency. Validated numerical simulations confirm these predictions, and some main findings on propulsive characteristics are as follows:

- The highest thrust and efficiency is obtained for $k = 2.5, h = 0.25$, among the parameters considered herein, where thrust and efficiency are increased by 53% and 15% with respect to single airfoil.
- Regarding the effect of phase angle, opposed plunge, i.e., $\phi = 180^\circ$, is found to be the most efficient among of all phase angles that are considered; $\phi = 0^\circ, \phi = 90^\circ, \phi = 180^\circ$, and $\phi = 270^\circ$, for both cases; $k = 2.5, h = 0.25$, and $k = 4, h = 0.15$.

- On the other hand, there is a force increase in vertical direction for $\phi = 90^\circ$ and $\phi = 270^\circ$ phase angles, whereas thrust and propulsive efficiency remains nearly the same as single airfoil.
- Finally, insignificance of the three dimensionality in the flow around plunging airfoils is exemplified for the cases $k = 2.5, h = 0.25$, and $k = 4, h = 0.15$ at phase angle $\phi = 180^\circ$.

ACKNOWLEDGMENTS

The authors are grateful for the use of the computing resources provided by The National Center for High Performance Computing (UHcM), under Grant Number 10752009 and the computing facilities at TUBITAK-ULAKBIM, High Performance and Grid Computing Center (TRUBA).

AUTHOR DECLARATIONS

Conflict of Interest

No potential conflict of interest is reported by the authors.

DATA AVAILABILITY

Experimental raw data were generated at (Trisonic Laboratory of Istanbul Technical University) the large scale water channel. Derived data supporting the findings of this study are available from the corresponding author upon reasonable request.

REFERENCES

- ¹K. D. Jones and M. F. Platzer, "On the use of vortex flows for the propulsion of micro-air and sea vehicles," *Symposium on Advanced Flow Management: Part A, Vortex Flows and High Angle of Attack for Military Vehicles*, 7–11 May 2001 (RTO-MP-069(I), Leon, Norway, 2001).
- ²K. Jones, B. Castro, O. Mahmoud, and M. Platzer, "A numerical and experimental investigation of flapping-wing propulsion in ground effect," AIAA Paper No. 2002-0866, 2002.
- ³I. H. Tuncer and M. Kaya, "Thrust generation caused by flapping airfoils in a biplane configuration," *J. Aircraft* **40**, 509–515 (2003).
- ⁴K. D. Jones, C. J. Bradshaw, J. Papadopoulos, and M. F. Platzer, "Bio-inspired design of flapping-wing micro air vehicles," *Aeronaut. J.* **109**, 385–393 (2005).
- ⁵K. Jones and M. Platzer, "Bio-inspired design of flapping-wing micro air vehicles—an engineer's perspective," AIAA Paper No. 2006-37, 2006.
- ⁶M. Kaya, I. Tuncer, K. Jones, and M. Platzer, "Optimization of aeroelastic flapping motion of thin airfoils in a biplane configuration for maximum thrust," AIAA Paper No. 2006-37, 2007.
- ⁷M. Kaya, I. H. Tuncer, K. D. Jones, and M. F. Platzer, "Optimization of flapping motion parameters for two airfoils in a biplane configuration," *J. Aircraft* **46**, 583–592 (2009).
- ⁸G. Dong and X. Lu, "Characteristics of flow over traveling wavy foils in a side-by-side arrangement," *Phys. Fluids* **19**, 057107 (2007).
- ⁹C. Han, H. Lee, and J. Cho, "Propulsive characteristics of dual fish-like foils," *J. Mech. Sci. Technol.* **22**, 171–179 (2008).
- ¹⁰J.-M. Miao, W.-H. Sun, and C.-H. Tai, "Numerical analysis on aerodynamic force generation of biplane counter-flapping flexible airfoils," *J. Aircraft* **46**, 1785–1794 (2009).
- ¹¹K. De Clercq, R. De Kat, B. Remes, B. van Oudheusden, and H. Bijl, "Flow visualization and force measurements on a hovering flapping-wing MAV'Delfly II," AIAA Paper No. 2009-4035, 2009.
- ¹²S. Deng, T. Xiao, B. van Oudheusden, and H. Bijl, "Numerical investigation on the propulsive performance of biplane counter-flapping wings," *Int. J. Micro Air Veh.* **7**, 431–439 (2015).
- ¹³W. B. Tay, B. Hester, and B. Van Oudheusden, "Analysis of biplane flapping flight with tail," AIAA Paper No. 2012-2968, 2012.
- ¹⁴Y. Shen and H. Cai, "Aerodynamic characteristics of multiple flapping wing configurations," *J. Vibroeng.* **18**, 1839–1848 (2016).
- ¹⁵Y. Bao, D. Zhou, J. Tao, Z. Peng, H. Zhu, Z. Sun, and H. Tong, "Dynamic interference of two anti-phase flapping foils in side-by-side arrangement in an incompressible flow," *Phys. Fluids* **29**, 033601 (2017).
- ¹⁶J. Zhu and B. Lei, "Effect of wing-wing interaction on the propulsive performance of two flapping wings at biplane configuration," *Appl. Biom. Biomech.* **2018**, 1–12.
- ¹⁷M. R. Amiralaei, H. Alighanbari, and S. M. Hashemi, "On the force signatures of a pair of multi-plunging airfoils," *Proc. Inst. Mech. Eng. Part G* **227**, 647–662 (2013).
- ¹⁸A. Gungor, M. Khalid, and A. Hemmati, "How does switching synchronization of pitching parallel foils from out-of-phase to in-phase change their wake dynamics?," *Phys. Fluids* **33**, 081901 (2021).
- ¹⁹J. Zhu and J. Zhang, "Power extraction performance of two semi-active flapping airfoils at biplane configuration," *J. Mech. Sci. Technol.* **34**, 175–187 (2020).
- ²⁰B. Erzinanlı and M. Sahin, "An arbitrary Lagrangian-Eulerian formulation for solving moving boundary problems with large displacement and rotations," *J. Comput. Phys.* **255**, 660–679 (2013).
- ²¹P. D. Thomas and C. K. Lombard, "Geometric conservation law and its application to flow computations on moving grids," *AIAA J.* **17**, 1030–1037 (1979).
- ²²Y. Saad, "A flexible inner-product preconditioned GMRES algorithm," *SIAM J. Sci. Comput.* **14**, 461–469 (1993).
- ²³A. J. Chorin, "Numerical solution of the Navier-Stokes equations," *Math. Comput.* **22**, 745–762 (1968).
- ²⁴R. Falgout, A. Baker, E. Chow, V. E. Henson, E. Hill, J. Jones, T. Kolev, B. Lee, J. Painter, C. Tong, P. Vassilevski, and U. M. Yang, "Users manual, hypre high performance preconditioners," Center for Applied Scientific Computing, Lawrence Livermore National Laboratory, Report No. ucll-ma-137155 dr, 2004.
- ²⁵S. Balay, K. Buschelman, V. Eijkhout, W. D. Gropp, D. Kaushik, M. G. Knepley, L. C. McInnes, B. F. Smith, and H. Zhang, "PETSc users manual," Mathematics and Computer Science Division, Argonne National Laboratory, Report No. anl-95/11, 2004.
- ²⁶G. Karypis and V. Kumar, "A fast and high quality multilevel scheme for partitioning irregular graphs," *Comput. Mech.* **20**, 359–392 (1998).
- ²⁷M. Sahin, "A stable unstructured finite volume method for parallel large-scale viscoelastic fluid flow calculations," *J. Non-Newtonian Fluid Mech.* **166**, 779–791 (2011).
- ²⁸M. Sahin, "Parallel large-scale numerical simulations of purely-elastic instabilities behind a confined circular cylinder in a rectangular channel," *J. Non-Newtonian Fluid Mech.* **195**, 46–56 (2013).
- ²⁹T. D. Blacker, S. Benzley, S. Jankovich, R. Kerr, J. Kraftcheck, R. Kerr, P. Knupp, R. Leland, D. Melander, R. Meyers, S. Mitchell, J. Shepard, T. Tautges, and D. White, "Cubit mesh generation environment user's manual," Sandia National Laboratories, Albuquerque, NM, 2004.
- ³⁰M. Percin, "Flow around a plunging airfoil in a uniform flow" (Master's thesis), Graduate School of Science and Technology, Istanbul Technical University, 2009.